Methods

Parasagittal cortical slices (300 μm thick, 30 degree angle) were obtained from Wistar rats (14–18 days old). Within this range, no correlation was found between the likelihood of coupling among FS cells and the animal age. The extracellular solution bathing the slices was kept at 32–33 °C and contained 125 mM NaCl, 2.5 mM KCl, 1.25 mM NaH_2PO_4, 1 mM $MgSO_4$, 2 mM $CaCl_2$, 26 mM $NaHCO_3$, 20 mM glucose, pH 7.4 (315 mOsm), and was continuously bubbled with a gas mixture of 95% O_2 and 5% CO_2.

Cell identification

Cells were selected and identified based on their physiology as well as their immunocytochemistry and morphology. Cells in layer V of the somatosensory and the visual cortices were initially selected according to their morphology using infrared differential interference contrast (IR-DIC) optics. Neurons lacking an apical dendrite with multipolar appearance were selected as FS cell candidates. To distinguish FS cells from other types of non-FS nonpyramidal cell we examined their response to near-threshold current injection. The distinguishing feature that we used to classify FS cells was the generation of high-frequency non-accommodating discharges of action potentials in response to near-threshold current injection[14–17]. We found that in FS cells ($n = 52$ cells), the mean interspike interval (ISI) in these near-threshold discharges was 8.0 ± 0.7 ms (range 2–23.7 ms), the coefficient of variation of the ISI was 0.085 ± 0.007, and the ratio of the second ISI to the first was 1.08 ± 0.02. Nonpyramidal neurons that lacked these characteristic discharges were classified as non-FS nonpyramidal cells. In this group, near-threshold discharges containing ⩾3 spikes had a mean ISI of 62.3 ± 10.8 ms (range 31.6–161.8), a coefficient of variation of the ISI of 0.483 ± 0.096, and a ratio of the second ISI to the first of 3.21 ± 1.00 ($n = 13$). FS cells also had the following characteristics: input resistance 92.4 ± 4 MΩ ($n = 52$), input time constant 8 ± 0.7 ms (measured by fitting the late phase of the response to a small current injection, $n = 50$), fast afterhyperpolarization amplitude −21.7 ± 0.6 mV (measured from the spike onset, $n = 52$), and spike width at threshold 0.6 ± 0.02 ms ($n = 52$). In addition, FS cells exhibited a remarkably high activity of spontaneous excitatory postsynaptic potentials (EPSPs). Pyramidal neurons were recognized by their characteristic morphology and pattern of spiking[16]. Glial cells were identified as having a resting potential more hyperpolarized than −80 mV, low input resistance, absence of synaptic inputs and inability to generate action potentials.

Morphology of neurons stained with biocytin was revealed by standard avidin-biotinylated-horseradish peroxidase complex (ABC, Vector Laboratories) and 3-3′ diaminobenzidine reaction. Fast-spiking cells successfully recovered were nonpyramidal neurons with aspiny radial dendrites. The axon originated in most cases from the upper part of the soma and branched locally with a predominantly horizontal orientation. Immunofluorescence methods were used to detect the presence of parvalbumin in biocytin-stained cells. We used mouse monoclonal antibodies against parvalbumin (Swant, #235, 1/5000), and secondary mouse IgG antibodies (Fab specific) conjugated with TRITC (tetramethylhodamineisothiocyanate) (Sigma, T-7782, 1/400). Biocytin-filled cells were detected using Neutravidin-Alexa 488 (Molecular Probes). Nine of twelve (75%) neurons classified as FS cells were immunopositive for parvalbumin. In contrast, none of ten non-FS cells tested for parvalbumin were immunopositive.

Recording and data analysis

Simultaneous somatic whole-cell recordings (Axopatch 200 A/B; Axon Instruments) were made using patch pipettes (2–4 MΩ) filled with a solution containing 130 mM K-methylsulphate, 6.3 mM KCl, 10 mM HEPES, 4 mM MgATP, 20 mM phosphocreatine(Na), 0.3 mM NaGTP, 10 mM EGTA and 0.3% mM biocytin, (pH 7.3, 295 mOsm). The liquid junction potential error was not corrected. The error in the estimation of the conductance between coupled cells produced by the series resistances was corrected[19]. Recordings from pairs of FS cells were obtained in the presence of DNQX (10 μM, RBI) to block AMPA/kainate receptor-mediated synaptic currents. Chemical synaptic transmission was studied by generating action potentials in the presynaptic neuron using brief pulses (3–5 ms) of suprathreshold currents. The reversal potential of the uIPSP was −56 mV ($n = 4$) and 10 μM bicuculline methiodide (a $GABA_A$-receptor antagonist) blocked the uIPSP generated by FS cells ($n = 3$). Voltage and current signals were filtered at 10 kHz and digitized at 16-bit resolution (National Instruments). The sampling frequency was 5–10 kHz. To synthesize 'natural' stimuli we convolved a Poisson train (2,000 Hz) with a waveform of an excitatory postsynaptic current (EPSC). The result was combined with the convolution of a Poisson train (1,000 Hz) and an IPSC waveform[30]. Trials were separated by 1 s. For each trial a different randomly generated Poisson train was used. The waveforms of the EPSC and IPSC used in the convolution were previously recorded unitary currents.

Data are given as mean ± s.e.m. Statistical analysis testing two-sample hypothesis was performed using unpaired, two-tailed Student's t tests. Differences were considered statistically significant if $P \leqslant 0.05$. Peaks in the cross-correlogram were considered significant if individual bins exceeded expected value by 2.5 standard deviations.

Received 27 April; accepted 23 August 1999.

1. Singer, W. & Gray, C. M. Visual feature integration and the temporal correlation hypothesis. *Annu. Rev. Neurosci.* **18,** 555–586 (1995).
2. Ritz, R. & Sejnowski, T. J. Synchronous oscillatory activity in sensory systems: new vistas on mechanisms. *Curr. Opin. Neurobiol.* **7,** 536–546 (1997).
3. Lytton, W. W. & Sejnowski, T. J. Simulations of cortical pyramidal neurons synchronized by inhibitory interneurons. *J. Neurophysiol.* **66,** 1059–1079 (1991).
4. Whittington, M. A., Traub, R. D. & Jefferys, J. G. R. Synchronized oscillations in interneuron networks driven by metabotropic glutamate receptor activation. *Nature* **373,** 612–615 (1995).
5. Cobb, S. R., Buhl, E. H., Halasy, K., Paulsen, O. & Somogyi, P. Synchronization of neuronal activity in hippocampus by individual GABAergic interneurons. *Nature* **378,** 75–78 (1995).
6. Michelson, H. B. & Wong, R. K. S. Synchronization of inhibitory neurones in the guinea-pig hippocampus in vitro. *J. Physiol. (Lond.)* **477,** 35–45 (1994).
7. Jefferys, J. G. R., Traub, R. D. & Whittington, M. A. Neuronal networks for induced '40 Hz' rhythms. *Trends Neurosci.* **19,** 202–208 (1996).
8. Strata, F. *et al.* A pacemaker current in dye-coupled hilar interneurons contributes to the generation of giant GABAergic potentials in developing hippocampus. *J. Neurosci.* **17,** 1435–1446 (1997).
9. Benardo, L. S. Recruitment of GABAergic inhibition and synchronization of inhibitory interneurons in rat neocortex. *J. Neurophysiol.* **77,** 3134–3144 (1997).
10. Tamás, G., Somogyi, P. & Buhl, E. H. Differentially interconnected networks of GABAergic interneurons in the visual cortex of the cat. *J. Neurosci.* **18,** 4255–4270 (1998).
11. Rinzel, J., Terman, D., Wang, X.-J. & Ermentrout, B. Propagating activity patterns in large-scale inhibitory neuronal networks. *Science* **279,** 1351–1355 (1998).
12. Zhang, Y. *et al.* Slow oscillations (≤1 Hz) mediated by GABAergic interneuronal networks in rat hippocampus. *J. Neurosci.* **18,** 9256–9268 (1998).
13. Kawaguchi, Y. & Kubota, Y. GABAergic cell subtypes and their synaptic connections in rat frontal cortex. *Cereb. Cortex* **7,** 476–486 (1997).
14. Kawaguchi, Y. & Kubota, Y. Correlation of physiological subgroupings of nonpyramidal cells with parvalbumin- and calbindinD28k-immunoreactive neurons in layer V of rat frontal cortex. *J. Neurophysiol.* **70,** 387–396 (1993).
15. Kawaguchi, Y. Physiological subgroups of nonpyramidal cells with specific morphological characteristics in layer II/III of rat frontal cortex. *J. Neurosci.* **15,** 2638–2655 (1995).
16. Galarreta, M. & Hestrin, S. Frequency-dependent synaptic depression and the balance of excitation and inhibition in the neocortex. *Nature Neurosci.* **1,** 587–594 (1998).
17. Angulo, M. C., Staiger, J. F., Rosier, J. & Audinat, E. Developmental synaptic changes increase the range of integrative capabilities of an identified excitatory neocortical connection. *J. Neurosci.* **19,** 1566–1576 (1999).
18. Cauli, B. *et al.* Molecular and physiological diversity of cortical nonpyramidal cells. *J. Neurosci.* **17,** 3894–3906 (1997).
19. Neyton, J. & Trautmann, A. Single-channel currents of an intercellular junction. *Nature* **317,** 331–335 (1985).
20. Hubel, D. H. Single unit activity in striate cortex of unrestrained cats. *J. Physiol.* **147,** 226–238 (1959).
21. Connors, B. W., Benardo, L. S. & Prince, D. A. Coupling between neurons of the developing rat neocortex. *J. Neurosci.* **3,** 773–782 (1983).
22. Peinado, A., Yuste, R. & Katz, L. C. Extensive dye coupling between rat neocortical neurons during the period of circuit formation. *Neuron* **10,** 103–114 (1993).
23. Sloper, J. J. Gap junctions between dendrites in the primate neocortex. *Brain Res.* **44,** 641–646 (1972).
24. Katsumaru, H., Kosaka, T., Heizmann, C. W. & Hama, K. Gap junctions on GABAergic neurons containing the calcium-binding protein parvalbumin in the rat hippocampus (CA1 region). *Exp. Brain Res.* **72,** 363–370 (1988).
25. Bragin, A. *et al.* Gamma (40–100 Hz) oscillation in the hippocampus of the behaving rat. *J. Neurosci.* **15,** 47–60 (1995).
26. Buhl, E. H., Tamás, G. & Fisahn, A. Cholinergic activation and tonic excitation induce persistent gamma oscillations in mouse somatosensory cortex in vitro. *J. Physiol. (Lond.)* **513,** 117–126 (1998).
27. Wang, X.-J. & Buzsáki, G. Gamma oscillation by synaptic inhibition in a hippocampal interneuronal network model. *J. Neurosci.* **16,** 6402–6413 (1996).
28. Traub, R. D., Whittington, M. A., Stanford, I. M. & Jefferys, J. G. R. A mechanism for generation of long-range synchronous fast oscillations in the cortex. *Nature* **383,** 621–624 (1996).
29. Bush, P. & Sejnowski, T. Inhibition synchronizes sparsely connected cortical neurons within and between columns in realistic networks models. *J. Comput. Neurosci.* **3,** 91–110 (1996).
30. Stevens, C. F. & Zador, A. M. Input synchrony and the irregular firing of cortical neurons. *Nature Neurosci.* **1,** 210–217 (1998).

Acknowledgements

We thank M. Chang for technical assistance. S.H. was supported by an NIH grant.

Correspondence and requests for materials should be addressed to S.H. (e-mail: shaul@nb.utmem.edu).

Two networks of electrically coupled inhibitory neurons in neocortex

Jay R. Gibson*, Michael Beierlein* & Barry W. Connors

Department of Neuroscience, Division of Biology & Medicine, Brown University, Providence, Rhode Island 02912, USA
** These authors contributed equally to this work*

Inhibitory interneurons are critical to sensory transformations, plasticity and synchronous activity in the neocortex[1,2]. There are many types of inhibitory neurons, but their synaptic organization is poorly understood. Here we describe two functionally distinct inhibitory networks comprising either fast-spiking (FS) or low-threshold spiking (LTS) neurons. Paired-cell recordings showed that inhibitory neurons of the same type were strongly interconnected by electrical synapses, but electrical synapses between

different inhibitory cell types were rare. The electrical synapses were strong enough to synchronize spikes in coupled interneurons. Inhibitory chemical synapses were also common between FS cells, and between FS and LTS cells, but LTS cells rarely inhibited one another. Thalamocortical synapses, which convey sensory information to the cortex, specifically and strongly excited only the FS cell network. The electrical and chemical synaptic connections of different types of inhibitory neurons are specific, and may allow each inhibitory network to function independently.

We recorded data from two common types of inhibitory interneurons of somatosensory neocortex, and tested the possibility that each type participates in a functionally distinct network defined by its synaptic inputs, intrinsic membrane properties, chemical and electrical synaptic interconnections, and output targets. Recordings were performed in layers 4 and 6 of rat barrel cortex using an *in vitro* slice that preserved connections between thalamus and barrel cortex[3] (Fig. 1a). We targeted neurons with large, usually vertically oriented somata (20–30 μm along the vertical axis, Fig. 1b) because these were most likely to be inhibitory[4]. Intrinsic membrane properties and synaptic inputs distinguished the two interneuron types[5–7]. Fast-spiking cells had narrow action potentials (a mean of 0.35 ms at half-amplitude), each with a deep, brief after-hyperpolarization, high firing rates (up to 320 Hz) when stimulated, and little or no frequency adaptation (Fig. 1c, mean rates after 600 ms were 97% of initial rates). When stimulated near threshold, FS cells often generated a slowly depolarizing voltage ramp before firing spikes at long latencies (up to 600 ms); stronger stimuli evoked spikes at short latencies. Low-threshold spiking cells had broader spikes (0.55 ms at half-amplitude),pronounced adaptation of firing frequency (mean rates after 600 ms fell to 39% of initial rates) and never generated a long delay before spiking (Fig. 1c). These LTS cells also displayed low-threshold spikes when depolarized from more negative potentials[6]. The two cell types had similar input resistances (FS, 58 ± 26 MΩ, $n = 127$; LTS, 71 ± 37 MΩ, $n = 40$; all data are expressed as mean ± s.d.).

Some interneurons in layer 4 were stained with biocytin or neurobiotin (FS, $n = 35$; LTS, $n = 5$). All had smooth or sparsely spiny dendrites, usually vertically oriented and bitufted, or multipolar, with dense axonal processes extending into layers 2/3 and 5. The morphologies of FS and LTS cells were not obviously different. Calcium-binding proteins and neuroactive peptides help to distinguish subtypes of γ-amino butyric acid (GABA)-mediated neurons

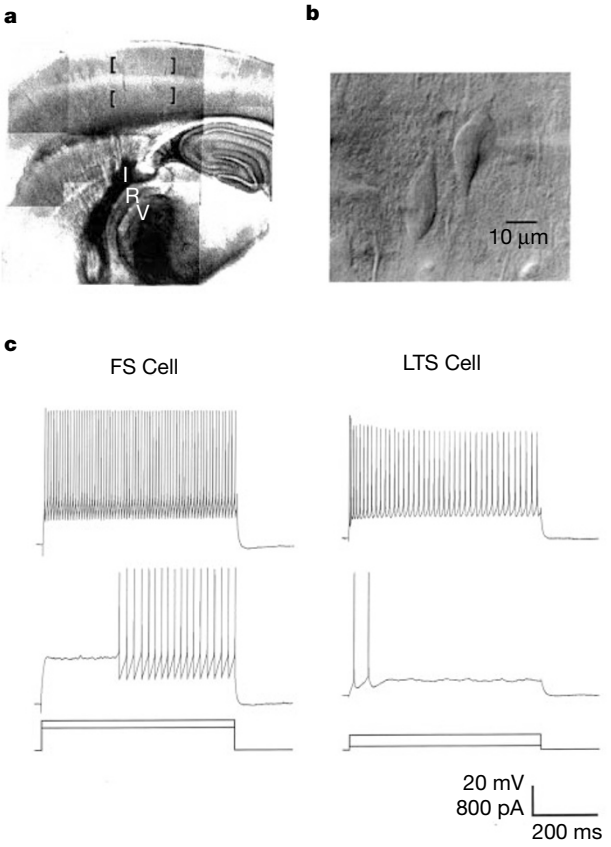

Figure 1 Two types of inhibitory interneurons. **a**, The thalamocortical slice as it appears in the recording chamber. Brackets mark the recording areas in layers 4 and 6 of neocortex. Thalamocortical afferents activated by stimulating the ventral basal nucleus of the thalamus (V) pass through the reticular nucleus of the thalamus (R) and the internal capsule (I). **b**, Video IR-DIC image of a pair of low-threshold spiking (LTS) cells just before recording. **c**, Current-clamp recordings from a fast-spiking (FS) cell (left) and an LTS cell (right) during injection of depolarizing current pulses of two intensities.

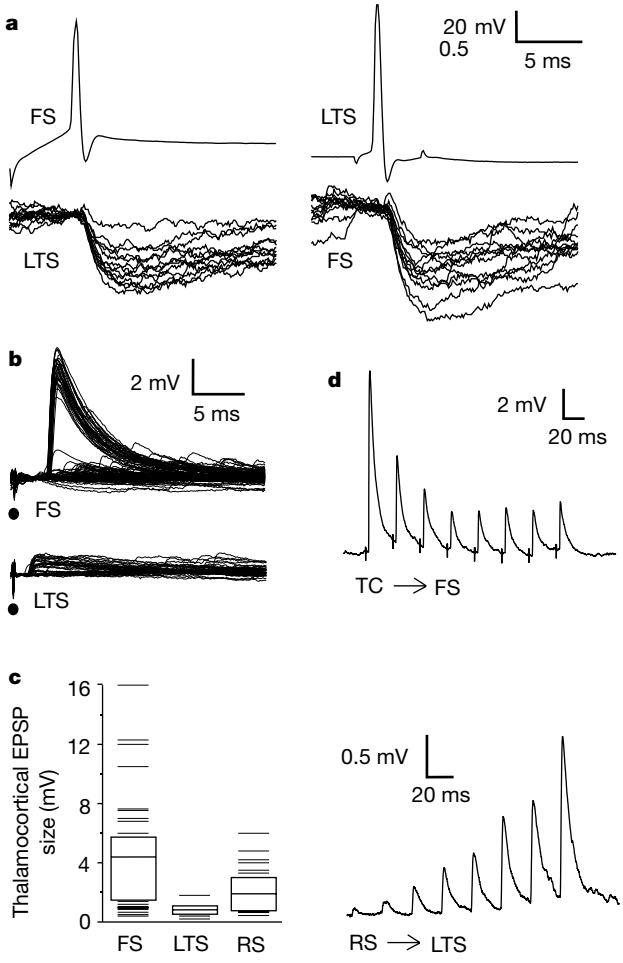

Figure 2 Chemical synaptic connections of inhibitory interneurons. **a**, Inhibitory synapses interconnecting FS and LTS neurons. During paired recordings, spikes in an FS cell evoked inhibitory postsynaptic potentials (IPSPs) in a neighbouring LTS cell (left); in a different pair, spikes in an LTS cell evoked IPSPs in an FS cell (right). In each case, 12 trials are illustrated from the postsynaptic cell, each aligned on the presynaptic spike that evoked it, and a single presynaptic spike is shown for each pair. **b**, Thalamocortical EPSPs evoked in an FS and an LTS cell with threshold stimuli. Multiple trials are overlaid. **c**, Summary of mean single-axon thalamocortical EPSP amplitudes, showing that FS cells responded more strongly than both LTS and regular-spiking (RS) cells. Boxes delineate the 25th and 75th percentiles, the line within the box is the sample mean, and lines outside the boxes plot the rest of the range ($n = 38$ FS, 8 LTS, 26 RS cells). **d**, Upper trace, thalamocortical (TC) inputs to FS cells strongly depress (average of 20 trials of suprathreshold stimuli applied at 40 Hz). Lower trace, intracortical excitatory inputs to LTS cells strongly facilitate (LTS cell response from presynaptic RS cell spikes evoked at 40 Hz; average of 20 trials).

Table 1 Electrical and chemical synapses between different types of neurons

Cell types	Total cell pairs	Chemical synapse	Reciprocal chemical synapses	Electrical synapse	Electrical and chemical synapses
FS ↔ FS	39	24	6	24	17
LTS ↔ LTS	13	2	0	11	1
LTS → FS	32	17	7	3	0
FS → LTS	32	11	7	3	0
RS ↔ RS	80	9	0	0	0
FTS/LTS → RS	71*	37	5	0	0
RS → FS/LTS	54*	22	5	0	0

Each row shows data from a particular type of neuronal pairing, with the number of cases that tested positively for a chemical synapse in one direction, a chemical synapse in two directions, electrical coupling, or both electrical and chemical synapses in at least one direction. FS, Fast-spiking cell (GABAergic); LTS, Low-threshold spiking cell (GABAergic); RS, Regular-spiking cell (glutamatergic). FS/LTS indicates that data from the two types were pooled. Arrows indicate the direction of the chemical synapses sampled.

*These represent the same sample of cell pairs, but in some cases glutamate receptors were blocked with AP5 and DNQX (see Methods), and thus the RS → FS/LTS connection could not be tested.

in neocortex[2]. When immunocytochemistry was combined with intracellular biocytin staining, 6 out of 14 FS cells were parvalbumin immunoreactive, and 3 out of 6 LTS cells were somatostatin immunoreactive. No LTS cells were positive for parvalbumin ($n = 4$), and no FS cells were positive for somatostatin ($n = 8$). This labelling specificity is consistent with previous electrophysiological studies of these cell types[6,7].

Paired recordings confirmed that these interneurons were inhibitory. Spikes in presynaptic FS and LTS cells evoked inhibitory postsynaptic potentials (IPSPs) in postsynaptic neurons of all types (Fig. 2a; Table 1); however, inhibitory interconnections were much more prevalent between pairs of FS cells (62%) than between pairs of LTS cells (15%). Both FS cells and LTS cells also inhibited regular-spiking (RS) cells, which are excitatory neurons[8]. Regular-spiking neurons occasionally made excitatory chemical synapses with each other (11%), but RS cells more frequently excited the interneurons (41%).

Excitatory inputs to the two interneuron networks differed in several ways. Thalamocortical axons convey sensory information to the neocortex by excitatory synapses in layers 4 and 5/6 (ref. 1). They also evoke rapid and powerful feedforward inhibition, and physiological[9,10] and anatomical[11] evidence suggests that FS cells may be involved. Single thalamocortical axons were stimulated, and excitatory postsynaptic potentials (EPSPs) were recorded (Fig. 2b). FS cells had, on average, the largest thalamocortical EPSPs (4.3 ± 3.7 mV, $n = 38$), whereas LTS cells had the smallest (0.8 ± 0.5 mV, $n = 8$; FS versus LTS, $p < 0.001$, t-test) (Fig. 2c). Thalamocortical responses were impossible to evoke in most LTS cells, even when neighbouring FS cells showed strong responses. The results indicate that LTS cells may receive weaker and far fewer thalamocortical inputs than FS cells. A less likely possibility is that afferents were differentially separated during slicing. Regular-spiking cells, the excitatory neurons, have thalamocortical responses of intermediate size (1.9 ± 1.5 mV, $n = 26$) (ref. 12). Thus, FS cells are very likely to be mediators of fast, feedforward thalamocortical inhibition.

Repetitive stimulation of thalamic axons at frequencies of 1–40 Hz produced strong depression of EPSPs in FS cells (Fig. 2d; mean EPSP amplitude fell by 73% after 8 stimuli at 10 Hz). Thalamocortical inputs to RS cells also depressed[12], but not as strongly as those to FS cells. Thalamic responses of LTS cells also clearly depressed, but they were too weak to measure. Both types of inhibitory cells received excitatory inputs from local RS cells (Table 1), and each had distinctive dynamics[7]. The RS–FS synapses depressed at all frequencies (mean EPSP amplitude fell by 46% after 8 stimuli at 10 Hz), whereas the synapses from RS to LTS cells markedly facilitated at frequencies above about 30 Hz (Fig. 2d; mean EPSP amplitude rose by 900% after 8 stimuli at 40 Hz).

The presence of dye coupling[13–15] and gap junctions[16,17] suggests that neocortical interneurons may be electrically coupled. To assess the electrical strength, specificity and functional consequences of coupling, we made paired recordings from neighbouring interneurons (<50 μm between somata). Among FS cell pairs, 62% were coupled (Table 1). Current steps applied to Cell 1 evoked voltage changes in Cell 2, and vice versa (Fig. 3a). The average attenuation of low-frequency voltages, or "coupling coefficient"[18], between FS cells was 0.07 ± 0.06 ($n = 24$). Action potentials attenuated much more than low-frequency voltages: the coupling coefficient for FS action potentials, when measurable, was 0.010 ± 0.006 ($n = 14$). We estimate that the coupling conductance between FS cells was 1.6 ± 1.3 nS (range of 0.4–5.5 nS, $n = 24$; Fig. 3b). Coupling strength was roughly equal in both directions, and showed no dependence on junctional voltage over ±40 mV. The coupling conductance accounted for up to one-third of the input conductance for the most strongly coupled FS cell pairs. The filtering characteristics of FS–FS cell coupling were tested with subthreshold current steps or sine waves of varying frequencies; coupling was strongest for steady voltages, and rolled off (decreased steeply) at high frequencies with a corner frequency of about 10 Hz. Among

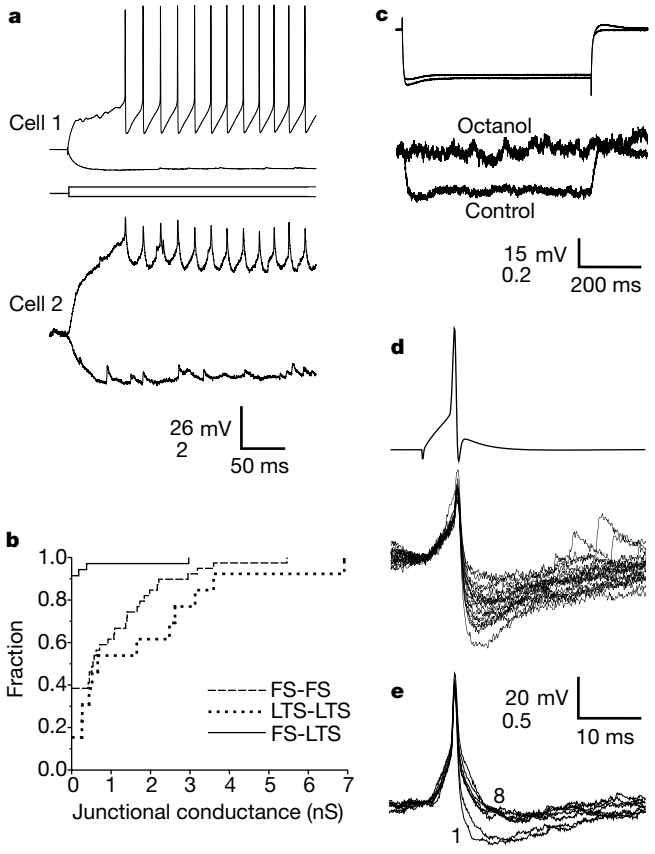

Figure 3 Electrical synapses between interneurons. **a**, Simultaneous recordings from two electrically coupled FS cells. Sequential current steps were applied to Cell 1 only (+400 pA, –200 pA). **b**, Cumulative frequency histogram of junctional conductances estimated from FS–FS ($n = 39$), LTS–LTS ($n = 13$) and FS–LTS ($n = 32$) neuron pairs. **c**, Octanol blocks electrical coupling. Average traces from two coupled FS cells under control conditions and in the presence of octanol (2 mM). Test current steps (–500 pA) were applied to the upper cell. **d**, Dual electrical–chemical synaptic connection between two FS cells. Spikes evoked in Cell 1 with short current pulses (single trace) triggered brief, sharp spikelets in Cell 2 followed by more prolonged and variable IPSPs (multiple trials overlaid). Postsynaptic responses were aligned on the presynaptic spike. **e**, Differential frequency sensitivity of electrical and chemical synaptic components. In an FS–FS pair (different from the pair in **d**), a 10-Hz train of 8 presynaptic spikes (not shown) evoked fast, reliable postsynaptic spikelets by electrical coupling, followed by IPSPs that were strongly depressed after the first 2 stimuli (first and last traces are numbered; each trace is the average of 15 trials).

LTS cell pairs, 85% were electrically coupled (Table 1), with an average coupling coefficient at low frequencies of 0.10 ± 0.09 ($n = 11$), and 0.015 ± 0.01 ($n = 7$) for action potentials. The average junctional conductance between LTS cells was 2.1 ± 2.3 nS (range 0.3–6.9 nS, $n = 11$; Fig. 3b). Strong coupling was observed at every age tested, including one pair of FS cells at postnatal day 26 and one pair of LTS cells at day 29. There was no correlation between junctional conductance and age. Although we demonstrated coupling only between pairs of cells, the prevalence of coupled pairs together with the spatial density of interneurons makes it likely that larger clusters of interneurons are electrically coupled. Electrical synapses were common only between interneurons of the same type (Table 1). Only 3 out of 32 mixed-type (FS–LTS) cell pairs were coupled, and 2 of those had very low junctional conductances (Fig. 3b). Furthermore, we never observed RS cells to be coupled to other RS cells or to interneurons.

Electrical coupling between neurons is usually mediated by gap junctions, which are clusters of intercellular channels formed from connexin proteins[19]. Alternative explanations, such as ephaptic or electrical field interactions[20], are very unlikely in this case because signal polarity was preserved and no transient capacitive coupling was observed. When electrically coupled interneurons were exposed to the gap junction blocker octanol[21] (1–2 mM), coupling was abolished in all cases (Fig. 3c; four FS–FS pairs, one LTS–LTS pair), and coupling recovered after washout of octanol in three of these. Octanol also nonspecifically suppressed action potentials, increased voltage noise and changed cell input resistance, but these effects did not account for the abolition of coupling.

Gap junctions often mediate intercellular chemical signalling[19], and dye coupling (the intercellular passage of a dye of low molecular weight) is often used as an indicator of gap junctions. We filled 24 interneurons with the dye neurobiotin. Although the dye-injected cells were all darkly stained, only one (an FS cell) had a clearly stained interneuron dye coupled to it. Dissociation between dye coupling and electrical coupling may have occurred because the diffusion rate of the dye through small, distally located gap junctions was too slow to allow the coupled cells to be seen. Alternatively, interneurons may be coupled through subtypes of connexins that form channels impermeable to the commonly used dyes[22]. A variety of connexins exist in the neocortex[23], but the connexin expression patterns of specific neuron types are not known. It is unlikely that the electrical coupling of interneurons is related to the developmental decline in dye coupling, primarily in excitatory cells, that has been observed[13,14].

Many FS cell pairs displayed both an electrical synapse and a chemical inhibitory synapse in at least one direction (Table 1). In such pairs, a spike in one cell evoked a biphasic voltage change in the coupled cell: a brief, short-latency, reliable depolarization communicated by the gap junction, and a slower, longer-latency, fluctuating IPSP triggered by the GABA-mediated synapse (Fig. 3d). Because the inhibitory synapses showed short-term depression and electrical connections did not, spike trains (0.5–40 Hz) in the first cell generated relatively constant depolarizations, but diminishing IPSPs, in the coupled cell (for example, 10 Hz in Fig. 3e). Thus, interneurons can communicate through both electrical and chemical synapses that display distinct polarities, timing and short-term dynamics.

Electrical coupling may serve to synchronize the electrical activity of neurons, as it does in the locus coeruleus[24] and inferior olive[25]. Interneurons of the cerebral cortex display various modes of synchronous and rhythmic activity, and both chemical and electrical synapses have been proposed as mediators of their synchrony[26,27]. We tested the synchronizing ability of electrical coupling by injecting subthreshold sine wave currents (0.5–100 Hz) into one neuron while holding a neighbouring coupled cell at a membrane potential just below spike threshold ($n = 9$, FS–FS pairs). Spiking in the second cell was easily entrained by the depolarizing peaks of the current applied to the first cell at frequencies up to 40 Hz (Fig. 4a). Alternatively, two coupled cells were induced to fire action potentials repetitively (50–100 Hz) with constant current injections. Chemical synapses were either blocked with drugs, or did not exist between the recorded neurons. In all cases (four FS–FS pairs, one LTS–LTS pair) sharply synchronous firing occurred (Fig. 4b).

Electrical coupling may contribute to the markedly sharp (±1 ms) spiking synchrony observed between pairs of FS cells *in vivo*[10]. Close synchrony among electrically coupled LTS cells is also predicted. The paucity of electrical connections between networks, however, should ensure that the fine patterns of FS and LTS spiking are independent. Some coordination between the two networks may occur through their reciprocal inhibitory connections. Several studies suggest that interneurons generate a variety of synchronous inhibitory rhythms in the neocortex[15,27,28]. Some of this variety may arise from the independent actions of electrically coupled LTS and FS networks, which are regulated by their differential sensitivity to neuromodulators[29,30]. □

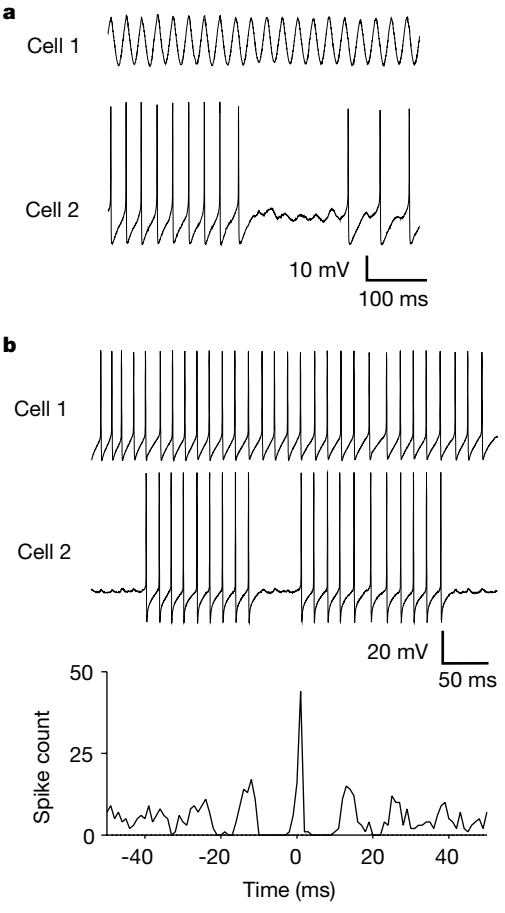

Figure 4 Electrical synapses coupling the spiking activity of two interneurons. **a**, During paired recordings of two FS cells, sinusoidal stimulus current (40 Hz) was applied to Cell 1 while Cell 2 was held just below spike threshold with constant current. Cell 2 fired phasically during many of the positive current peaks in Cell 1. **b**, In a different pair of FS cells, spikes were elicited by simultaneously applying steady depolarizing current to both cells. The traces represent a sample of a longer trial from which a cross-correlation of action potentials was calculated. Cell 1 was the reference for the correlation. The cross-correlogram below shows strong, sharp (±2 ms) synchrony.

Methods

Slice preparation and recording

Thalamocortical slices[3] 250–450 μm thick were obtained from Sprague–Dawley rats aged P14–P21 (unless otherwise noted). Slices were incubated at 32 °C for 1 hr, and then held at 32 °C during recordings. The bathing solution contained 126 mM NaCl, 3 mM KCl,

1.25 mM NaH_2PO_4, 2 mM $MgSO_4$, 26 mM $NaHCO_3$, 10 mM dextrose and 2 mM $CaCl_2$, saturated with 95% O_2/5% CO_2. Micropipettes were filled with 135 mM K-gluconate, 4 mM KCl, 2 mM NaCl, 10 mM HEPES. 0.2–4 mM EGTA, 4 mM ATP-Mg, 0.3 mM GTP-Tris, 0.5–10 mM phosphocreatine-Tris (pH 7.25, 295 mOsm). All recordings were made in current clamp mode, with infrared-differential interference contrast (IR-DIC) visualization using a Zeiss Axioskop and a CCD camera (Hamamatsu).

Extracellular stimuli were biphasic current pulses lasting 200 μs, typically at about 50 μA (10–120 μA), applied through microwires. Thalamic responses were measured at membrane potentials of –60 to –70 mV, with 50 μM DL-2-amino-5-phosphopentanoic acid (AP5) in the bath to block N-methyl-D-aspartate (NMDA) receptors. In a few experiments (see Table 1) 20 μM of the AMPA receptor antagonist 6,7-dinitroquinoxaline-2,3-dione (DNQX) was also added.

Thalamocortical responses were collected with a conservative 'minimal response' protocol: threshold stimulus intensities evoked EPSPs (up to 100 trials) presumed to be generated by single thalamocortical axons. Most EPSP failures probably arose from failure of presynaptic axon spiking; incrementing stimulus intensity abolished failures without increasing EPSP size and shape. Thalamocortical responses were discarded from cells in which IPSPs were detected.

Junctional conductance

Estimating the junctional conductance[18] assumed a model of two isopotential neurons and a single junction. Junctional conductance and the two cell input conductances were solved from simultaneous equations, using the injected currents and voltage responses of each cell. Coupling conductances were estimated for each direction of current flow in a cell pair; differences were usually small, and reported values are the average of the two. The model does not account for complexities arising from junctions on dendritic or axonal cables, and it does not incorporate nonlinear membrane properties.

Anatomical labelling

Neurobiotin or biocytin (4 mg ml^{-1}) was added to the normal filling solution in some recordings. Slices were fixed in 4% paraformaldehyde (sometimes with 0.2% picric acid) in 0.1 M phosphate buffer, transferred to 30% sucrose, resectioned to 80 μm, and reacted with avidin-biotin-peroxidase (Vector). In dye-coupling experiments with neurobiotin, cells were recorded for 1–1.75 hr and, in about half of the cells, current steps were applied in an effort to maximize dye delivery.

Some cells underwent a fluorescent double-labelling immunocytochemical protocol for biocytin and either parvalbumin or somatostatin, using two different fluorophores. Slices were first stained using monoclonal antibodies for either parvalbumin (Sigma, S-3171, diluted 1:400, visualized by CY_3-conjugated goat anti-mouse IgG (Jackson Immuno Research), or somatostatin (S-309, gift of R. Benoit, Montreal, Canada, visualized by CY_3-conjugated donkey anti-rabbit IgG (Chemicon). Biocytin was visualized using 7-amino-4-methylcoumarin-3-acetic acid (AMCA)-conjugated streptaviden (Jackson Immuno Research). Immunonegative cells could result from genuine scarcity of the marker in a cell, or could reflect damage to a recorded cell.

Received 18 May; accepted 26 August 1999.

1. Somogyi, P., Tamas, G., Lujan, R. & Buhl, E. H. Salient features of synaptic organisation in the cerebral cortex. *Brain. Res. Rev.* **26,** 113–135 (1998).
2. Jones, E. G. GABAergic neurons and their role in cortical plasticity in primates. *Cerebral Cortex* **3,** 361–372 (1993).
3. Agmon, A. & Connors, B. W. Thalamocortical responses of mouse somatosensory (barrel) cortex in vitro. *Neuroscience* **41,** 365–379 (1991).
4. Simons, D. J. & Woolsey, T. A. Morphology of Golgi-Cox-impregnated barrel neurons in rat SmI cortex. *J. Comp. Neurol.* **230,** 119–132 (1984).
5. Thomson, A. M. & Deuchars, J. Synaptic interactions in neocortical local circuits: dual intracellular recordings in vitro. *Cereb. Cortex* **7,** 510–522 (1997).
6. Kawaguchi, Y. & Kubota, Y. GABAergic cell subtypes and their synaptic connections in rat frontal cortex. *Cereb. Cortex* **7,** 476–486 (1997).
7. Reyes, A. & Sakmann, B. Target-cell-specific facilitation and depression in neocortical circuits. *Nature Neurosci.* **1,** 279–285 (1998).
8. Connors, B. W. & Gutnick, M. J. Intrinsic firing patterns of diverse neocortical neurons. *Trends Neurosci.* **13,** 99–104 (1990).
9. Agmon, A. & Connors, B. W. Correlation between intrinsic firing patterns and thalamocortical synaptic responses of neurons in mouse barrel cortex. *J. Neurosci.* **12,** 319–329 (1992).
10. Swadlow, H. A., Beloozerova, I. N. & Sirota, M. G. Sharp, local synchrony among putative feed-forward inhibitory interneurons of rabbit somatosensory cortex. *J. Neurophysiol.* **79,** 567–582 (1998).
11. Staiger, J. F., Zilles, K. & Freund, T. F. Distribution of GABAergic elements postsynaptic to ventroposteromedial thalamic projections in layer IV of rat barrel cortex. *Eur. J. Neurosci.* **8,** 2273–2285 (1996).
12. Gil, Z., Connors, B. W. & Amitai, Y. Efficacy of thalamocortical and intracortical synaptic connections: quanta, innervation, and reliability. *Neuron* **23,** 385–397 (1999).
13. Connors, B. W., Benardo, L. S. & Prince, D. A. Coupling between neurons of the developing rat neocortex. *J. Neurosci.* **3,** 773–782 (1983).
14. Peinado, A., Yuste, R. & Katz, L. C. Extensive dye coupling between rat neocortical neurons during the period of circuit formation. *Neuron* **10,** 103–114 (1993).
15. Benardo, L. S. Recruitment of GABAergic inhibition and synchronization of inhibitory interneurons in rat neocortex. *J. Neurophysiol.* **77,** 3134–3144 (1997).
16. Sloper, J. J. & Powell, T. P. Gap junctions between dendrites and somata of neurons in the prime sensori-motor cortex. *Proc. R. Soc. Lond. B* **203,** 39–47 (1978).
17. Bozhilova-Pastirova, A. & Ovtscharoff, W. Structure of the synaptic junctions in the rat sensorimotor cortex: freeze-etching study of neuronal gap junctions. *Neurosci. Lett.* **201,** 265–267 (1995).
18. Bennett, M. V. L. in *Handbook of Physiology, Section 1: The Nervous System, Part I* (eds Brookhart, J. M. & Mountcastle, V. B.) 357–416 (American Physiological Society, Bethesda, 1977).
19. Dermietzel, R. & Spray, D. C. Gap junctions in the brain: where, what type, how many and why? *Trends Neurosci.* **16,** 186–192 (1993).
20. Jefferys, J. G. R. Nonsynaptic modulation of neuronal activity in the brain: electric currents and extracellular ions. *Physiol. Rev.* **75,** 689–723 (1995).
21. Johnston, M. F., Simon, S. A. & Ramon, F. Interaction of anesthetics with electrical synapses. *Nature* **286,** 498–500 (1980).
22. Veenstra, R. D. Size and selectivity of gap junction channels formed from different connexins. *J. Bioenerg. Biomembr.* **28,** 327–337 (1996).
23. Nadarajah, B., Jones, A. M., Evans, W. H. & Parnevelas, J. G. Differential expression of connexins during neocortical development and neuronal circuit formation. *J. Neurosci.* **17,** 3096–3111 (1997).
24. Christie, M. J., Williams, J. T. & North, R. A. Electrical coupling synchronizes subthreshold activity in locus coeruleus neurons *in vitro* from neonatal rats. *J. Neurosci.* **9,** 3584–3589 (1989).
25. Mann-Metzer, P. & Yarom, Y. Electrotonic coupling interacts with intrinsic properties to generate synchronized activity in cerebellar networks of inhibitory interneurons. *J. Neurosci.* **19,** 3298–3306 (1999).
26. Michelson, H. B. & Wong, R. K. Synchronization of inhibitory neurones in the guinea-pig hippocampus in vitro. *J. Physiol. (Lond.)* **477,** 35–45 (1994).
27. Jefferys, J. G., Traub, R. D. & Whittington, M. A. Neuronal networks for induced '40 Hz' rhythms. *Trends Neurosci.* **19,** 202–208 (1996).
28. Buhl, E. H., Tamas, G. & Fisahn, A. Cholinergic activation and tonic excitation induce persistent gamma oscillations in mouse somatosensory cortex in vitro. *J. Physiol. (Lond.)* **513,** 117–126 (1998).
29. Kawaguchi, Y. & Shindou, T. J. Noradrenergic excitation and inhibition of GABAergic cell types in rat frontal cortex. *J. Neurosci.* **18,** 6963–6976 (1998).
30. Xiang, Z., Huguenard, J. R. & Prince, D. A. Cholinergic switching within neocortical inhibitory networks. *Science* **281,** 985–988 (1998).

Acknowledgements

We thank S. Patrick for technical assistance, Y. Amitai and M. Bear for comments on the manuscript, and R. Benoit for gifts of anti-somatostatin antibodies. This work was supported by a fellowship to J.R.G. from NIH and a grant to B.W.C. from NIH.

Correspondence and request for materials should be addressed to B.W.C. (e-mail: Barry_Connors@Brown.edu).

Complex lipid determines tissue-specific replication of *Mycobacterium tuberculosis* in mice

Jeffery S. Cox*, Bing Chen*, Michael McNeil† & William R. Jacobs Jr*

** Howard Hughes Medical Institute, Department of Microbiology and Immunology, Albert Einstein College of Medicine, Bronx, New York 10461, USA*
† Department of Microbiology, Colorado State University, Ft. Collins, Colorado 80523, USA

Tuberculosis is the leading cause of death in the world resulting from a single bacterial infection[1]. Despite its enormous burden on world health, little is known about the molecular mechanisms of pathogenesis of *Mycobacterium tuberculosis*. Bacterial multiplication and concomitant tissue damage within an infected host, including experimentally infected mice, occurs primarily in the lungs—the favoured niche of *M. tuberculosis*[2]. Although it has been proposed that the distinctive cell wall of *M. tuberculosis* is important for virulence, rigorous genetic proof has been lacking. Here, using signature-tagged mutagenesis, we isolated three attenuated *M. tuberculosis* mutants that cannot synthesize or transport a complex, cell wall-associated lipid called phthiocerol dimycocerosate (PDIM) which is found only in pathogenic mycobacteria[3,4]. Two mutants have transposon insertions affecting genes implicated in PDIM synthesis; the third has a disruption in a gene encoding a large transmembrane protein required for proper subcellular localization of PDIM. Synthesis and transport of this complex lipid is only required for growth in the lung; all three mutants are unaffected for growth in the liver and spleen. This clearly shows that a lipid is required for *M. tuberculosis* virulence.

To identify *M. tuberculosis* genes that are required for growth *in vivo*, we adopted the signature-tag mutagenesis (STM)[5] scheme to screen multiple 'inoculum' pools of 48 random transposon mutants